UNIVERSITY OF BIRMINGHAM

System Design for the Facilitation of Rydberg Stark Deceleration of Strontium-88 Atoms

Keith Taylor 1540418
Partner: *Ed Lewis*
Supervisors: *Dr Yogeshwar Kale* and *Dr Yeshpal Singh*
School of Physics and Astronomy
March 2019

Word Count: 8346

A design for a proof of concept portable Rydberg-Stark decelerator was created to prepare atoms before trapping. The system was designed to use two photon excitation to create Rydberg atoms of the order $n = 50 - 70$ and then decelerate from 350 to 10ms^{-1} using a 2D array of electrodes housed in an evacuated monolithic cell.

CONTENTS

1. INTRODUCTION

The ability to manipulate the motion of atoms is advantageous in many fields of study across scientific research, branching into Chemistry as well as Physics. This report will focus primarily on the design of an experiment to manipulate the translational motion of Strontium-88 atoms using electric field gradients, the Stark effect and Rydberg states. Any atom which has been excited to a high principle quantum number is said to be in a Rydberg state. The pervasiveness of these states throughout all atoms and molecules combined with the way they can be used in conjunction with other physical theories makes them an extremely useful tool. Creating ultracold atoms has opened doors and lead to advancements in a variety of fields. Diatomic molecules have a more complex internal structure and lack of electric dipole moment making them more difficult to decelerate by methods other than Rydberg-Stark deceleration. Their more complex internal structure also makes them more interesting[1].

As will be made clear later, the interaction between Rydberg atoms and inhomogeneous electric fields is beneficial to decelerating and eventually trapping atoms and molecules. High values of atomic principle quantum number combined with electric fields leads to large electric dipole moments *and* an extension in the fluorescence lifetime of atoms, and therefore in interaction time. Various experimental techniques have been developed to take advantage of both of these facts to aid in the deceleration and trapping of atoms and molecules.

Decelerated Rydberg atoms and molecules have numerous applications. They have been essential in high resolution millimetre wave spectroscopy used to determine the ionisation energies of Hydrogen atoms and its isotopomers[2] and in determining the hyperfine structure of Hydrogen atoms in Rydberg states[3]. Many of the experiments using decelerated Rydberg atoms and molecules are actually in the field of chemical physics and in many cases the improved interaction lifetime has been the main factor in the improving frequency resolution.

The electronic transition frequency of atoms can be utilised for atomic clocks. Just as a grandfather clock uses a pendulum, or a quartz clock uses a crystal, atomic clocks use the electronic transition frequency of an atom as their resonator. The current standard is 9192631770 oscillations of the radiation corresponding to the energy transition between two hyperfine energy levels of the ground state of Caesium-133 at absolute zero[4]. This radiation has a wavelength of 3.26cm meaning it belongs in the microwave regime.

One of the main motivations for this project was to create a system which could decelerate ^{88}Sr atoms in preparation for an atomic clock operating in the optical regime. Once trapped, the electronic transition frequency can be measured precisely. The narrower the linewidth, the lower the uncertainty in the measurement. Since the Caesium standard of the second was set, the uncertainty in atomic clocks has reached unprecedented levels. The radiation corresponding to ^{88}Sr's energy transition for atomic clocks has a wavelength which places it in the optical regime. Optical clocks are approaching the quantum noise limit[5][6].

Atomic clocks are integral in many technologies which rely on synchronisation. Global Navigation Satellite Systems (GNSS) such as GPS rely on several atomic clocks in each satellite for accurate triangulation. A larger uncertainty in the time taken for a signal to travel between a GPS device on Earth and a GPS satellite results in a larger error in positioning. The theoretical uncertainty of GPS time is 14 nanoseconds[7]. If the speed of light is 3×10^8 ms^{-1}, this leads to a positional uncertainty of approximately 4 metres, as this is how far light could have travelled in this time. Atomic clocks are also used in testing physical theories and any system which requires time synchronisation such as traffic systems, air traffic control or a financial system like the stock market.

The ultimate goal is to create a system which decelerates atoms in a smaller space than any of its counterparts: regular multistage Stark deceleration, Zeeman

deceleration or optical Stark deceleration[8]. A smaller system of deceleration reduces the size and weight of the system it is a part of. This makes the entire system more portable and therefore more versatile. Size and weight are particularly important factors to minimise when it comes to space based systems like a GNSS.

2. THEORY

I. Zeeman Deceleration

A Zeeman decelerator decelerates atoms using a magnetic field. The magnetic field interacts with any atoms containing a magnetic dipole moment. An atom has a magnetic dipole moment if it's total angular momentum is not zero. The application of a magnetic field splits previously well defined spectral lines into a hyperfine structure. This is known as the Zeeman effect[9]. A magnetic field exerts a torque on the atoms which results in magnetic potential energy, $U(\theta)$, given in Equation 1 where μ is the magnetic dipole moment and B is the magnetic field.

$$U(\theta) = -\mu B \tag{1}$$

If the magnetic dipole moment as a result of the angular momentum L is $\mu = -\frac{e}{2m_e}L$ then the hyperfine structure is displaced from ground by δE given in Equation 2, where m_l is the z component of the angular momentum, assuming the magnetic field is in the z direction.

$$\Delta E = -\frac{e}{2m_e}LB = -m_l\frac{e\hbar}{2m}B \tag{2}$$

This uniform splitting is the Zeeman effect. By using multiple stages and current pulses to create inhomogeneous magnetic fields all the kinetic energy can be removed from the atoms.

II. Stark Deceleration

The Stark effect[10], utilised by Stark deceleration is analogous to the Zeeman effect previously described, only it applies to the electric dipole moment. When an atoms are subjected to an external electric field their previously sharp and defined energy levels are split. The field polarises the atom, giving it an electric dipole moment, this is what the electric field then interacts with. The magnitude of the total angular momentum, rather its sign determines the dipole moment. As a result the energy levels split proportional to the quantum numbers relating to full and half integer spins, $J+1$ and $J+\frac{1}{2}$ respectively.

When the atoms energy levels are split they can be placed into two categories: high field seekers and low field seekers. Placement in either category is independent of any property of the atom but rather depends on the electric field strength and whether the atom is static or tumbling. If an atom is mostly aligned with the field it becomes a high field seeker and vice-versa if it is mostly anti-parallel it will be a low-field seeker. Static (non-tumbling) atoms are either aligned or anti-parallel and are categorised as such, although they tend to align, as this is most favourable. Tumbling atoms rotate quickly through the aligned direction and slowly through the antiparallel direction as it is least favourable. Since tumbling atoms spend more time antiparallel they will become low-field seekers.

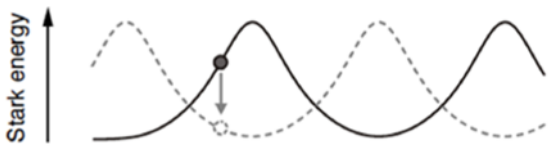

Fig. 1. Graph showing the varying stark energy through space, depicting high and low field seekers travelling with and against the gradient.

The high field seekers in the beam moving into an area of strong electric field will gain kinetic energy. The low field seekers will lose kinetic energy as depicted in Figure 1. By using time dependent inhomogeneous the electric field gradient is continuously switched so that the low field seekers are kept, continuously incrementally losing kinetic energy. Vice-versa, high field seekers can be continually decelerated, as long as an appropriate switching sequence is chosen.

The degree of shifting and splitting of energy levels is determined by the size of the electric dipole moment. The electric dipole moment is proportional to the

principle quantum number. This is taken advantage of by Rydberg-Stark deceleration.

III. Rydberg States

Any atom or molecule can be excited. In other words, any atom or molecule can have its state raised from low *n* principle quantum number to a high *n*. Physically, a high *n* state is an atom with at least one extremely excited electron. As it becomes more excited, its orbit increases, as does its ability to couple with an electric field. These high *n* states are known as Rydberg states. The energy of these states is given by Equation 3[11], the Rydberg formula to the first order. The energies of each Rydberg state converge as they follow the Rydberg formula. The energy associated with this limit is E_{ion}. R_m is the Rydberg constant after correction for the reduced mass, h and c are the Planck constant and the speed of light respectively.

$$E_{nl} = E_{ion} - \frac{hcR_m}{(n-\delta_l)^2} \tag{3}$$

The Rydberg formula is used to predict the wavelength of radiation emitted from an internal energy transition. Equations 4, 5, 6 and 7 detail the derivation of Equation 3.

$$\frac{1}{\lambda} = RZ^2(\frac{1}{n_1^2} - \frac{1}{n_1^2}) \tag{4}$$

Equation 4 shows the Rydberg Formula, where λ is the emitted radiations wavelength, *R* is the Rydberg constant, *Z* is the atomic number and n_1 and n_2 are the transition energy levels. The energy level of the n^{th} level of an atom with one electron can be written as:

$$E_{nl} = \frac{RZ^2}{n^2} \tag{5}$$

The energy level of the n^{th} level for any atom therefore can be written as:

$$E_{nl} = \frac{R_{eff}}{n_e^2} \tag{6}$$

Where R_{eff} is the effective Rydberg constant and n_e is the effective quantum number. δ_l is the quantum defect dependent on the orbital angular momentum number *l* of the Rydberg electron. It is essentially the amount that the ion core is screened. δ_l decreases as *l* increases. When $\delta_l = n - n_e$ and the energy levels are taken from below an ionisation limit, Equation 6 becomes:

$$E_{nl} = E_{ion} - \frac{R_{eff}}{(n-\delta_l)^2} \tag{7}$$

Rydberg atoms with low l can quickly predissociate. This means they transition from a stable excited state to an unstable one without spontaneous emission. If *l* is higher and the Rydberg atom has a stable ion core, the lifetime of these atoms is longer. Previously the lifetime of such states had been the limiting factor in experiments, as mentioned earlier.

Equation 8 shows the Stark shift as a result of an electric field. Just as a Zeeman shift results from a magnetic field interacting with a magnetic dipole, the Stark energy shift is a result of the electric dipole moment. As shown by Equation 9, a higher principle quantum number makes Rydberg atoms more sensitive to electric fields. This is particularly taken advantage of in Rydberg-Stark deceleration.

$$E_{Stark} = \mu_{elec} F \tag{8}$$

$$\mu_{elec} = \frac{3}{2} n^2 e a_0 \tag{9}$$

IV. Rydberg-Stark Deceleration

Rydberg atoms electric dipole moment scales with n^2 (Equation 9). Atoms with very high n are therefore very sensitive to electric fields. This makes them prime candidates for use in Stark deceleration.

Rydberg-Stark deceleration is a more applicable and versatile tool than other forms of deceleration since *all* atoms and molecules can be photoexcited to a Rydberg state. Multi-stage Stark or Zeeman deceleration have to rely on the base electric or magnetic dipole moment being enough.

V. Strontium-88

Investigations into Rydberg states initially began with Johann Balmer, then Johannes Rydberg[12], followed by Niels Bohr. A full explanation for the observed Rydberg spectra was finally produced by Wolfgang Pauli in 1926. Each of these focused on transitions in Hydrogen. Gradually focus shifted to other types of atoms, particularly alkali metals[13]. When alkali metals are excited into a Rydberg state their singular outer electron sees the rest of the atom essentially as a point charge and so it becomes hydrogen-like.

More recently, alkaline earth metals, such as Strontium have been investigated[14]. This group of atoms is interesting because they have two valence electrons, which allows a variety of combinations of Rydberg states, with the possibility of interactions between those states. Figure 2[15] shows various transitions to Rydberg states via double or triple photon excitation. This report focuses on the the two photon excitation up to 5sns,nd $^1S_0$, $^1D_2$.

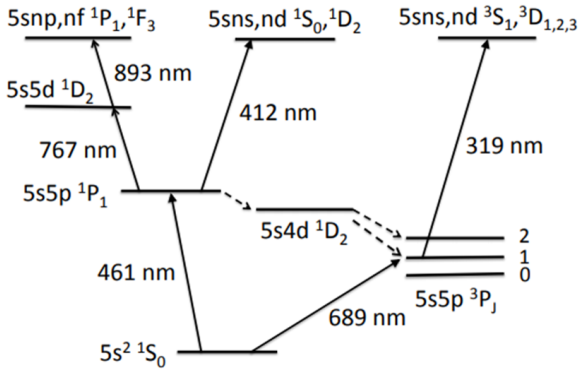

Fig. 2. Various transitions for producing single and triple Rydberg states

^{88}Sr is the most abundant of Strontium's four naturally stable isotopes. Of these four, only ^{87}Sr is fermionic, meaning it has an odd-integer spin which leads to a ground state hyperfine structure which in turn leads to unnecessary complications in spectra. The other three are bosonic, so they have no spin and no complications. The energy and therefore the wavelength of each excited state can be calculated using Equation 10 and known values[17]. Equation 10 is Equation 3 specific to ^{88}Sr.

$$E_{tot} = E_{ion} - \frac{R_{Sr}}{n} \tag{10}$$

$$E_{tot} = E_1 + E_2 \tag{11}$$

The total energy for the transition to this state can be calculated using Equation 10 rearranged for E_{tot}.

For example, if $n = 50$ was desired and if $R_{Sr} = 109736.627\text{cm}^{-1}$ and $E_{ion} = 45932.198\text{cm}^{-1}$ then $E_{tot} = 45888.303\text{cm}^{-1}$. This value is the total for the energy transition. This corresponds to a wavelength of 217.920nm. This ultra-violet laser was not available, however due to it's frequent use in other systems involving Strontium, like Zeeman decelerators, a 461nm laser was available.

Using Equation 11 the constituent energy's for two photon excitation can be calculated. the energy of the known first excited state, E_1, ($^1P_1$) is subtracted from E_{tot}. $E_1 = 21698.452\text{cm}^{-1}$ which corresponds to a wavelength of $\lambda_1 = 460.862$nm. Therefore $E_2 = 24189.851\text{cm}^{-1}$ which corresponds to a wavelength of $\lambda_2 = 413.397$nm. Each energy value is in units of cm^{-1} because energy is inversely proportional to wavelength, following $E = \frac{hc}{\lambda}$.

As the principle quantum number increases, the energy tends to that of the ionisation energy. So when $n^2 >> R_{Sr}$, $\lambda_2 = 412.648$nm. The closer the laser can scan to this value, the higher the Rydberg state can be achieved. The limiting factor in this method will be the resolution of the EIT signal. Both Lochhead[16] and Millen[17] struggled to resolve the EIT spectrum above $n \approx 70$ so it was decided that a Rydberg state of $n \approx 50 - 70$ should be aimed for.

VI. Laser locking

Rydberg states are achieved via two step photoexcitation using a blue 461nm laser and a violet 413nm laser. Stabilisation techniques are necessary to lock each of the two lasers. Fluctuations in laboratory conditions leads to small laser frequency drifts which are enough

to change the mode . In order to lock the lasers, a variety of methods can be used. They each incorporate a form of spectroscopy and a feedback system in order to identify the resonant frequency and then maintain it. Much research and interest has been placed in laser frequency locking over the past several decades. Methods include polarisation spectroscopy[18][19] (PS), saturated absorption spectroscopy[21][22] (SASpect) and electromagnetically induced transparency (EIT).

Spectroscopy is the study of any spectra produced by the interaction between light and matter. Absorption spectroscopy relies on the quantised nature of energy levels in atoms and the random scattering of radiation following the de-excitation of an excited atom or molecule. When a laser passes through a sample of atoms, the atoms will absorb and emit exactly enough energy to excite electrons. They will then emit this energy in a random direction, leading to a loss of this frequency in the resulting energy spectra of the laser. This allows the identification of particular energy levels within the atom or molecule.

A major limiting factor in spectroscopy work is Doppler broadening. The widths of spectral lines increase due to the distribution of velocities in the sample. SASpect and EIT can circumvent this limit and are known as sub-Doppler methods of spectroscopy.

VII. Polarisation Spectroscopy

Initially demonstrated by Wieman and Hänsch[20], Polarisation spectroscopy uses a circularly polarised pump beam, passing through a sample of atoms, to determine the polarisation change of a counter propagating linearly polarised probe beam. It is also a form of sub-Doppler spectroscopy.

A strong circularly polarised pump beam passes through a sample. This induces optical anisotropy in the sample which leads to Birefringance. A weaker, linearly polarised probe beam is then passed through the sample. Due to the induced optical changes by the pump beam, it's polarisation is changed. This is measured using two photodiodes, see Figure 9. One method is to retro-reflect one beam is to become the counter propagating beam on itself. If the beam passes initially through a $\frac{\lambda}{2}$ it is linearly polarised. Upon reflection if it passes through through a $\frac{\lambda}{8}$ wave plate twice, it is circularly polarised.

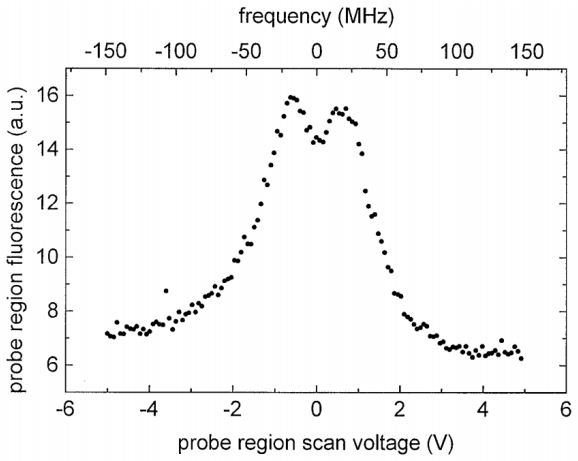

Fig. 3. Example of a resultant frequency spectrum from saturated absorption spectroscopy[21]

In the case of ^{88}Sr, the pump beam saturates the transition from ground state $^1S_0$ to a $m_J = \pm 1$ sub level of $^1P_1$. The rotation in polarisation caused by the resulting Birefringance can measured by splitting the beam and subtracting the two circular components from each other.

VIII. Saturated Absorption Spectroscopy

Removing the polarisation from PS converts to SASpect. A specifically tuned strong pump beam saturates a transition in a sample. The counter propagating probe beam's absorption is decreased due to the saturation. This results in a dip in intensity, as pictured in Figure 3. Although both beams will interact with atoms with a variety of speeds they will only both interact with atoms which are stationary relative to both of them. This results in no cases of Doppler broadening.

IX. Electromagnetically Induced Transparency

Transparency in a medium can be induced by preventing the absorption of incident energy on the medium. The physical repercussions of EIT, a quantum mechanical phenomenon, is a change in the optical properties

of a medium. The lack of absorption in the probe beam renders the medium transparent.

Transparency can be induced by causing the probability amplitudes of energy transitions to interfere destructively. This can happen if the environment is set up correctly. The first requirement is that the system is configured in three levels: either lambda, ladder or vee, see Figure 4.

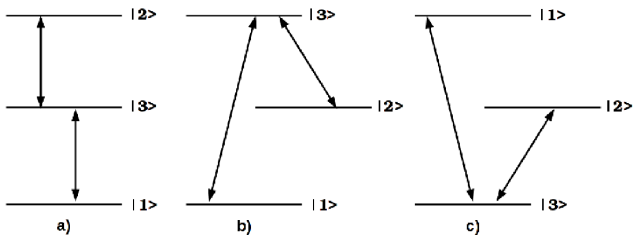

Fig. 4. Configurations of energy levels where EIT can be achieved. a) Ladder b) Lambda c) Vee

The second requirement is that one of the transitions must be non-allowed. This means it cannot be induced by an oscillating electric field. When two counter propagating beams differ by a non-allowed transition then interference occurs. This interference is quantum rather than optical and is the result of interfering transitions. For example, in Figure 4a), the ladder configuration is shown. The probability amplitude of state three depends on the probability amplitudes of states one and two. The probability amplitudes of states one and two are equal in magnitude and opposite in sign. When the counter propagating beams are coherent, destructive interference occurs so that the probability amplitude of state three is zero. This happens because the total probability of a state is calculated by summing the probability amplitudes, rather than probabilities themselves. Since the amplitudes can be negative this can lead to a total cancellation.

3. Method

The first step in spectroscopy and deceleration of atoms is to create an ultra high vacuum. In the case of this experiment, no physical setup existed, so one needed to be created. A system needed to be created which allowed for the distribution of strontium atoms from a source, space for spectroscopy and excitation of the atoms, space for deceleration and space to trap the atoms. The entire set-up also needed to be evacuated, to a degree.

Due to the ambitious aims of the project as a whole, the mains tasks became to lock the lasers and design the experimental equipment necessary to house and carry out this experiment. It was realised at an early stage that designing and implementing a magneto-optical trap was beyond what could be achieved in the given timescale. Primary goals of at least achieving vacuum and seeing fluorescence were set. Secondary and tertiary goals were set as achieving SASpect and EIT and then decelerating the atoms. Given the time allowed for the project, the learning curve required for some of the tasks and the lead times on components, the primary goals are the most that could be achieved. The hope is that the time spent on this project will be a good setup for future students taking this project.

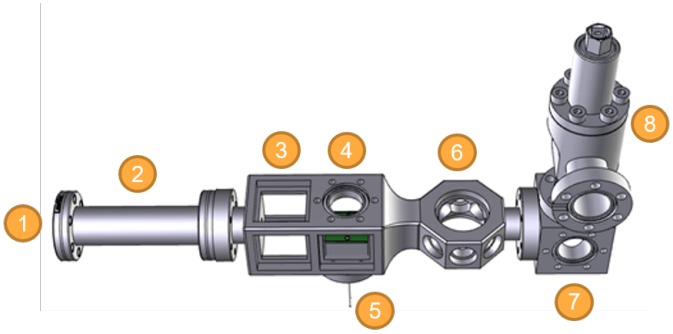

Fig. 5. Experimental setup, picture from Inventor assembly. 1- ^{88}Sr entrance point; 2- CF16 nipple; 3- spectroscopy stage; 4- PCB housing/ deceleration stage; 5- electrical feedthrough; 6- trapping/ velocity measurement stage; 7- six way cube; 8- All-metal valve.

The full set up is shown in Figure 24 and Appendix VII. The central cell and Surface-electrode PCB are custom built, the rest of the parts are standard vacuum components. One of the motivations behind this project was to make progress towards a portable decelerating device. The length of the setup in Figure 24 is 263mm with the deceleration occurring at 128mm over a length of 20mm.

I. Cell Design

The larger of the two custom parts necessary for this project was the monolithic cell. This cell needed to fit to CF16 standard flanges and have space for an atomic beam to pass through the centre while being excited from external lasers and decelerated internally. It was decided that a one-piece (monolithic) cell was preferable to several separate components for two reasons. Firstly, a flush, one piece cell will reduce the possibility of a vacuum leak compared to several gasket sealed component parts. Secondly, in the interest of portability, a monolithic cell takes up less space than the four parts it would need to replace it. Ideally, the cell would be manufactured from titanium. This would ensure structural integrity during the clamping for indium sealing of windows and also while under vacuum. Titanium's hardness and strength would also mitigate worries about which gaskets can be used without damaging the cell itself. Due to the high cost of titanium, a heat treated aluminium cell was decided on instead.

The following design was modified from an existing core and procured. Figure 6 shows the design and Figure 19 shows the final product.

There were several manufacturing and materials options considered before settling on selectively melting from aluminium. CNC machining and 3D printing were the first considerations. Due to the complex topology of the cell, CNC machining would not have been able to effectively create the design to an acceptable degree of accuracy. Numerous overhangs in the design would have created a large deal of post 3D printing work in order to finish the cell suitably. The workshop was unusually inundated throughout the year. As a result the lead time was several months so the selective melting route was chosen.

The first section of the cell is for spectroscopy. All four spaces in this section will be closed with square windows and indium sealed. The process for indium sealing will be covered later. The middle section houses the PCB and will be sealed on two sides with indium

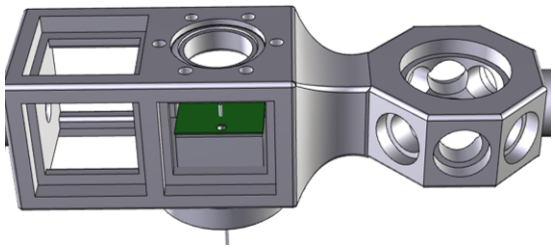

Fig. 6. Monolithic cell, Inventor model

sealed square windows, on the underside by an electrical feedthrough and a sapphire view port from above. The final stage of the cell is versatile in its utility. The end goal for this section is to serve as a MOT. It could also easily be used for velocity measurements prior to trapping. The openings here will be closed by six 12.5mm diameter and two 25mm diameter circular windows.

The full assembly of the monolithic cell and attached parts must be completed in a certain order. The ceramic separator and PCB had to be glued down with Torr seal initially. To ensure the PCB is completely inline with the atomic beam, a small right angle is used on both sides while the Torr seal is setting. The electrical feedthrough can then be attached, the wires trimmed and soldered to the PCB using a particular vacuum resilient solder. Once this has been completed, any and all of the 14 windows can be sealed, view ports and electrical feedthrough's can be attached and the cell can be fit into the full setup.

Lead solder is vacuum compatible up to around 10^{-5} Torr. Ideally, for spectroscopy, an ultra-high vacuum or better is necessary (10^{-9} - 10^{-12} Torr). The choice of solder (and other materials and components in this assembly) is important in order to avoid outgassing as much as possible. Outgassing occurs when a dissolved or trapped gas is released from a material. This can be prompted by the onset of a vacuum. The gas released from a material can then proceed to condense and coat surrounding surfaces, compromising the vacuum and localised equipment. Outgassing can be avoided by choosing a vacuum compatible material and by baking

the system in order to remove any trapped liquids. The LIGO project makes public its proceedings when it comes to fabrication and construction of PCB's for use in ultra-high vacuum (UHV)[23]. For soldering the PCB to the electrical feedthrough in this project, a slight variation on the LIGO suggestion was used. This variation was only dictated by stock availability in the lab. LIGO uses a Sn96.5Ag3.0Cu0.5 composition, this project used a Sn95.8Ag3.5Cu0.7 solder.

Spectroscopy and trapping require different degrees of vacuum. A lower pressure in the MOT section of the cell, by definition, reduces the number of hot atoms and other residuals. Too many hot atoms and residuals negatively affect the lifetime of the MOT. A useful feature of custom building the monolithic cell was the ability to incorporate differential pumping into the design. If the two pressures, the distance between the two spaces and the pumping speed are known, the conductance can be calculated using Equation 12.

$$\frac{P_1}{P_2} = \frac{C}{C+S} \tag{12}$$

Where P_1 and P_2 are the two pressures, C is conductance and S is pumping speed. In this case P_1 and P_2 were 10^{-6} and 10^{-9} respectively, S was 100L/s and conductance was therefore 0.1L/s.

Using this value of conductance, Equation 13[24] can be used to calculate the diameter of the hole required for differential pressure.

$$C = \frac{12.1d^3}{l} \tag{13}$$

Where d is the diameter and l is the length of the hole. When l was 2.1cm (from schematics), d was calculated to be 0.26cm. This feature was incorporated into the design, but due to an error was not included. An insert was created with the correct dimensions, as an improvised solution, it is shown in Appendix IV. Due to factors unconsidered by this model, this figure can only be considered as an order of magnitude calculation.

II. Surface-Electrode Decelerator

The second custom part for this project was the printed circuit board used as a surface-electrode decelerator (SED) to decelerate the Rydberg atoms. This PCB had to be vacuum compatible, small enough to fit inside the monolithic cell and capable of creating electric field potential wells. The final product is shown in Figure 20. An investigation of previous work brought to light a large variation in possible deceleration and trapping techniques. Two cylindrical rods, parallel with the atomic beam have been used to deflect atoms using time independent fields[25][26]. The standard template uses a series of electrodes, which the atomic beam then passes over or through[27]. 2D, 3D[28], on-axis and off-axis[29] variations of this approach have all been used. PCB's for use in day to day operations are usually made from some variation of woven fibreglass with a flame resistant epoxy resin as binding. The most common grade is FR-4 is an excellent insulator with little to no water absorption. FR-4's versatility makes it an excellent choice in many environments in a electrical applications. However, the porous nature of FR-4 make it likely to have gas trapped during manufacturing. As a result they will outgas in a vacuum. The material of choice for LIGO's PCB's in UHV is Rogers RO3003, a ceramic-filled PTFE composite[23]. Using a ceramic material rather than fibreglass and epoxy is beneficial because it reduces the amount of outgassing and therefore improves the quality of the vacuum. Due to excessive lead times on acquiring RO3003, Rogers RO4350b was substituted[30], a ceramic laminate material. If time was not an issue, RO3003 would have been used, this would have alleviated any concerns with outgassing.
A design for the PCB based off of one of S.D. Hogan's experiments[31] was produced, see Figure 7. The initial design had two sets of 10 electrodes which interlocked. Each side is connected to a coated hole on either side which can then be attached to the electrical feedthrough. It is essentially 10 pairs of electrodes in a 2D array. Each electrode is 0.5mm wide with the centre to centre spacing set to 1mm. These dimen-

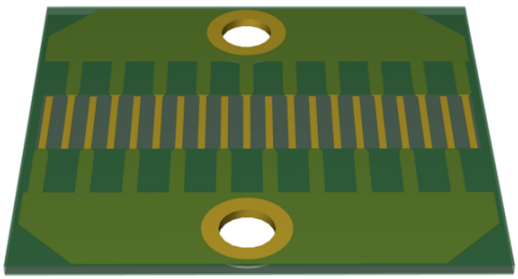

Fig. 7. Initial design of SED. A 2D array of 20 electrodes, evenly spaced. Dimensions: 20.60x18.62x1.6mm

sions were initially set in Hogan's paper to match the characteristics of the atomic beam. Hogan and Meek's[32] designs differ crucially from this schematic as they use six separate connections, each applying a different oscillating potential to create a set of travelling traps every three electrodes. In this schematic, two alternating potentials are applied, resulting in a different electric field gradient.

The potential gradient created by these electrodes necessary to decelerate Rydberg ^{88}Sr atoms was calculated using the distance available to decelerate, the initial velocity of the atoms and the desired velocity. Using Equation 14, where v is final velocity, u is initial velocity, s is distance and a is acceleration and using the values $v = 10\text{ms}^{-1}$, $u = 350\text{ms}^{-1}$, $s = 0.025\text{m}$ gives a deceleration of $2.4 \times 10^6\text{ms}^{-2}$.

$$a = \frac{v^2 - u^2}{2s} \tag{14}$$

As previously mentioned, the change in kinetic energy of the excited atom is equal to the change in Stark energy. This interaction is governed by the strength of the electric dipole moment which is in turn governed by the principle quantum number. Equation 9 showed the relationship between the electric dipole moment, μ_{elec}, the principle quantum number n, the electronic charge e and the atomic radius, a_0.

In this case, $n = 70$, $e = 1.6 \times 10^{-26}$ C and $a_0 = 5.3 \times 10^{-11}$ m for ^{88}Sr. This results in an electric dipole moment of $\mu_{elec} = 6.2 \times 10^{-26}$ Debye.

The electric field gradient, ∇F, can be calculated from Equation 15. m is the mass and a and μ_{elec} are as described previously.

$$\nabla F = \frac{ma}{\mu_{elec}} \tag{15}$$

When $m = 2.4 \times 10^{-25}$ Kg, $a = -2.4 \times 10^6$ ms^{-2} and $\mu_{elec} = 6.2 \times 10^{-26}$ Cm, the required gradient is $\nabla F = -6 \times 10^6$ Vm^{-1}.

After a great deal of searching, a PCB manufacturing company was found which could produce the PCB as the design specified.

To predict what the electric field gradients produced by the atoms would look like and how they would affect atoms, a simulation was produced. This simulation also allowed the comparison of this model to Hogan's model. The output of the various simulations are shown in the results section of this report.

III. Cleaning Procedure

Once a vacuum system part was procured and delivered, it was cleaned and baked. There are several stages to the cleaning process necessary to create a good standard of ultra high vacuum. There is the initial clean, an initial bake and a post assembly bake.

The initial clean:

1) Clean with soapy distilled water, submerge and leave in the ultra-wave machine for 15 minutes at 50 °C.
2) Clean with acetone, submerge and leave in the ultra-wave machine for 15 minutes at 50 °C.
3) Clean with iso-propanol, submerge and leave in the ultra-wave machine for 15 minutes at 50 °C.

Gloves were worn at all times and changed if contaminated. For wiping off excess liquids, Kimtech wipes were used. Inbetween steps, all parts were placed on UHV foil. Post clean and pre bake, each part was wrapped in this foil.

Initial baking was done under vacuum at 200 °C for 48 hours (including warm up and cool down). This removed excess moisture from the parts to allay outgassing. The PCB's delivery was delayed and the

system was preemptively baked. Due to the reabsorption of moisture over the week long delay, all parts were re-baked again.

Once the setup is fully assembled, another bake will occur at a 100 °C. The reason for the lower temperature is to avoid damaging the PCB and solder. The solder has a melting point of 217 °C and the PCB has a temperature tolerance of up to 150 °C, however it seemed wise to stay well within the tolerances.

IV. Vacuum Sealing

Finding a vacuum is the next stage of this project. All parts are in place to do this, but other deadlines dictated how much time could be spent in pursuit of a good vacuum. 14 windows are to be closed by indium sealing, one electrical feedthrough attached using a silver gasket and a sapphire view port attached, also with a silver gasket.

Indium sealing works through cold welding, compressing the indium creates an air tight chemical bond between the window and the cell. The quality of the seal is dependent on the quality and cleanliness of the indium, the cleanliness of the surface and the thickness of the indium. Therefore steps must be taken to prepare the surface and indium for sealing.

Initially, both the surface and indium wires are cleaned with acetone and then dried. Ideally the wire would also be cleaned with 50% hydrochloric acid in order to etch the surface of oxidation. The wire is then fitted to the seal and the windows placed above. At the point where the two ends of the wire cross there is to be a good overlap without excess wire. 3D printed separators are placed between the windows and the compression flanges provided by the workshop. The flanges are then slowly and evenly screwed tighter, compressing the window into the seal.

Sealing the electrical feedthrough and view port is theoretically very similar, only substituting indium for an appropriate gasket. The suitability of a gasket only depends on the relative hardness of the cell and the gasket. If the gasket is harder than the cell material it is being compressed into, the cell will be damaged. Therefore any material softer than heat treated aluminium can be used.

V. Optical Design

The aim was to use two photon excitation to bring the atoms to a principle quantum number of 70. This was to be achieved using a blue 461nm laser first to facilitate the $5s^2\ {}^1S_0$ to $5s5p\ {}^1P_1$ transition. Then a violet 413nm laser to facilitate the $5s5p\ {}^1P_1$ to $5sns,nd\ {}^1S_0$, ${}^3D_{1,2,3}$. As mentioned previously, in order to combat frequency drifting, both of these lasers were to be locked using various spectroscopic methods to lock in the relevant energy transitions. This process was to be split into three stages, blue laser locking with polarisation spectroscopy, violet laser locking with EIT and finally excitation using the same two lasers. While the monolithic cell was being made a cell at 1×10^{-10} Torr was used, supplying atoms via a dispenser at 5A of current.

The process for building up this excitation platform

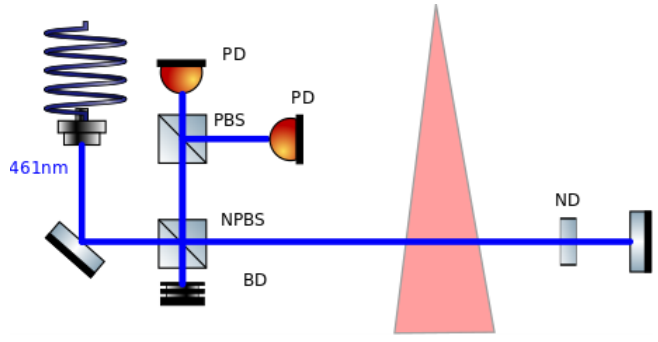

Fig. 8. Optical arrangement for Saturated absorption spectroscopy.

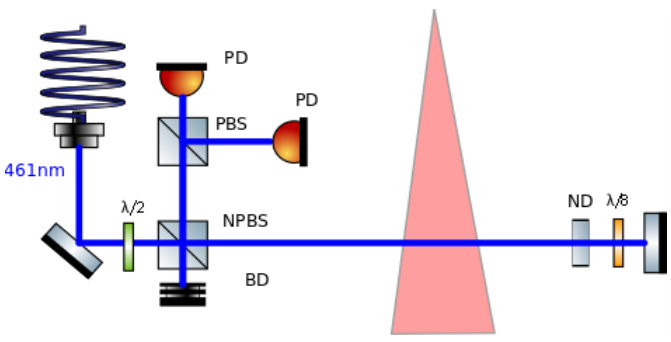

Fig. 9. Optical arrangement for polarisation spectroscopy.

was to start by finding fluorescence. This was achieved relatively quickly by changing the current and voltage of the input to navigate the different modes and scan over the known frequency of 650.5038 THz. Once this frequency had been found it was kept with difficulty. Gradual frequency drift quickly caused the frequency mode to hop away from resonance. The constant resetting due to this instability made progression here slow. Various techniques were attempted in order to stabilise the frequency, including varying the temperature, adjusting the feedforward and using a feedback system used by previous students. These had little effect. A video of fluorescence was taken, several frames are shown in Appendix V.

Once fluorescence had been found and the frequency mode was relatively stable, an attempt at saturated absorption spectroscopy was made. A Toptica DL PRO HP laser using the appropriate laser controller was used, allowing variation in current, voltage and temperature (temperature was kept at 21 °C). By connecting the receiving photodiodes to an oscilloscope (triggered by the laser controllers digital trigger), the broadened linewidth of transition should have been visibly oscillating as the laser scanned over resonance and the atoms fluoresced. The $^1S_0$ to $^1P_1$ transition has a linewidth of 32 MHz. As a result of Doppler broadening, this is an underestimate. This signal appeared to be non-existent at first so a top-down search of the equipment was made to inspect for faults or mistakes in the setup which would lead to a weak or lack of signal. No mistakes were found. A de-noising circuit utilising an op-amp was incorporated into the system with little effect. Again, a sweep of the system was carried out to ensure all connections were working. In addition to this, various efforts to increase the interaction of the beam with the atoms were attempted. These included optimising the gain on the photodiode, retro reflecting the beam back through the atoms, widening the beams cross section and focusing the beam on the photo diode.

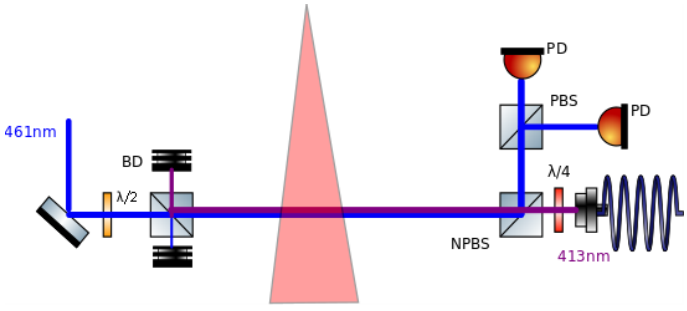

Fig. 10. Optical arrangement for electromagnetically induced transparency.

Had the signal been found and stabilised, the set-up for saturated absorption spectroscopy could have begun. This would have involved retro reflecting the 461nm laser back onto itself to act as a the pump and probe beam. The probe beam would then have been split into two photo diodes. The next step would have been to add a $\frac{\lambda}{8}$ wave plate just before retro reflection and a $\frac{\lambda}{2}$ wave plate at the start of the 461nm laser to convert SASpect into polarisation spectroscopy. Figures 8 and 9 show the optical arrangement for SASpect and polarisation spectroscopy. This design is based on the Groswasser[33] set up to maximise the use of space. Frequency modulated spectroscopy was not used because it needs expensive electro-optical modulators.

The final stage would have been to incorporate the 413nm laser for use in electromagnetically induced transparency. The 413nm laser would counter propagate through the 461nm laser. The 461nm laser would then be split off into two photodiodes. Figure 10 shows the optical arrangement for EIT.

The final adjustment would have been to re-reflect both beams to excite the Strontium beam. The full optical setup would have looked like the schematic shown in Appendix VI.

As a result of not finding the signal for SASpect, a switch to fluorescence spectroscopy was made. This simply involved moving the photo diode out of the main beam path and to a right angle above or below the fluorescing atoms. By focusing the light (solely from fluorescence) onto the photo diode, using 'averaging' on the oscilloscope and increasing the power of the laser, a signal was seen, Figure 11. With the known value of the separation between thee peaks, 124.5

MHz[17] the linewidth was calculated to be 188 MHz. The disparity between this broadened linewidth and the natural linewidth of 32 MHz justified the use of SASpect.

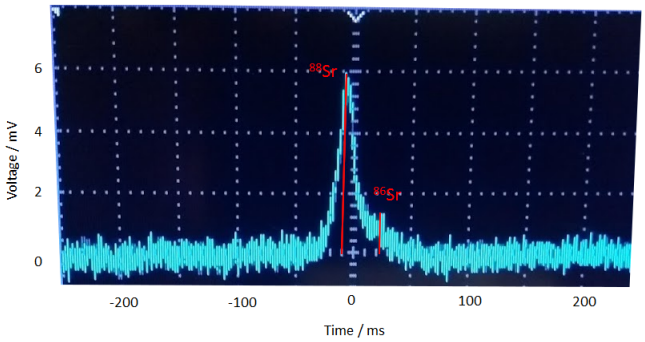

Fig. 11. Fluorence signal showing spectral peaks for ^{88}Sr and ^{86}Sr.

VI. Final Design

All the necessary parts are in place and ready to be assembled, as shown in Appendix I. The vacuum schematic is shown in Figure 24 and Appendix VII and the full optical set up is shown in Appendix VI. Because the project had not been run before the only parts already in stock were the Strontium source and the all-metal valve. The monolithic cell had been mostly designed, only requiring some adaptations. The learning curve for adapting the design for the monolithic cell, designing the PCB, waiting for quotes and lead times from company's and then issues with procurement meant that insufficient time was allocated to build the setup.

4. Results and Interpretations

I. Cell

All parts necessary to build the vacuum set up are in place. Each part was designed or modified successfully. Appendicies II and III show the physical copy's of the custom designs. Appendix I shows all the physical parts in an exploded view, ready to be assembled.

The monolithic cell was successfully designed to incorporate a differential pumping hole of 2.5mm diameter, When an error resulted in this part missing from the physical design, a new insert was designed to be incorporated.

Some flaws in the monolithic cell design came to light on arrival of the physical copy. A combination of some edges being too thin and manufacturing tolerances lead to small gaps in the edges of the first chamber. The windows in this section sit inside the indented area and as a result, the gaps should not be an issue.

In addition, the cell is made from aluminium which has subsequently been heat treated to improve its hardness. This was a necessary precaution to ensure the cell would not deform while under compression for vacuum sealing. The heat treating also increased the brittleness of the cell leaving it liable to flaking. An immediate solution to this problem would be to ask the workshop to give the cell a better surface finish. A future solution to this issue would be to use titanium as the main material of the cell. Although these issues have the potential to complicate the process of building the system, none of them will completely negate the effectiveness of the cell. Overall the design is good, but it is expensive to execute it well.

II. Spectroscopy

The progress in finding saturated absorption spectroscopy and electromagnetically induced transparency was slow. An inability to amplify the signal to a usable level meant that progress was halted before SASpect was found. fluorescence was found relatively quickly, several frames from a video are show in Appendix V. Switching to fluorescence spectroscopy yielded a clear signal as seen in Figure 11. The broadened linewidth of this line justified the reasoning behind wanting to use sub-Doppler spectroscopy methods.

III. PCB

A number of simulations were produced to predict the electric fields produced by this PCB and the one designed by Hogan. The simulations also provided an insight into how effective the PCB's might be in decelerating the atoms and what the atoms flight paths might look like. Variations in whether the fields are

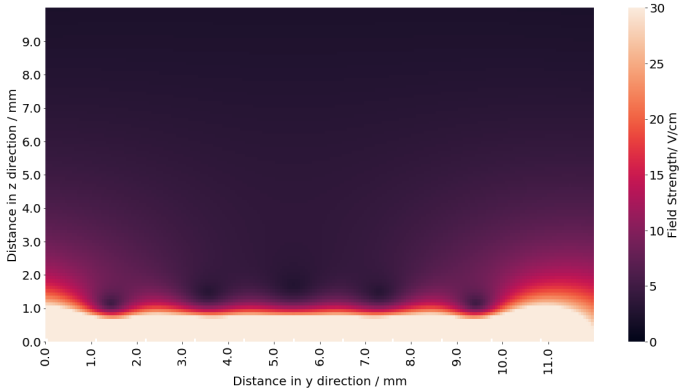

Fig. 12. Electric field above our PCB at 30 V, side view

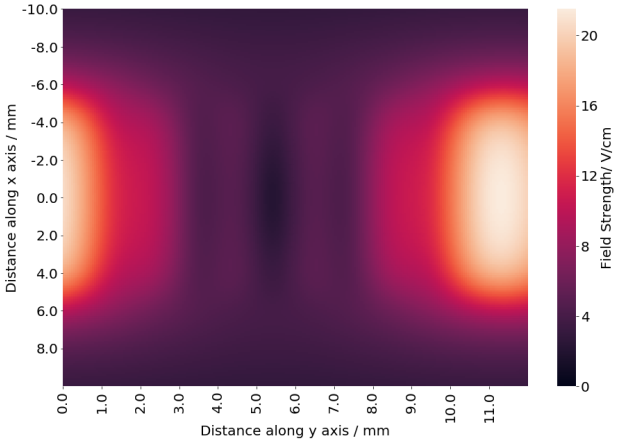

Fig. 13. Electric field above our PCB at 30 V, plan view

time dependent or static, electric field strength and the initial position of the atom were all possible. As was visualising the velocity distribution over the course of deceleration.

Interpreting these simulations is a good indicator of any outstanding flaws or problems in the design of the PCB.

The first simulation was of the fields themselves. In Figures 12 and 13 and Figures 14 and 15 the mapping of the fields above the electrodes of ours and Hogans PCB's respectively. The main disparity between the two is that Hogan's PCB uses six alternating potentials, see Figure 16, whereas ours uses two static ones. Six is clearly better as it provides greater versatility in the shapes of fields that can be produced, however the problem of finding six connections via the electrical feedthrough was not overcome.

Another important difference to consider is the difference in the lowest point of each of the two sets of potentials. The lowest on our PCB is at approximately 1mm above the base of the PCB. For Hogan's the lowest is at the base itself. This small difference affects the downward force on the atoms. Too much force in the direction of the PCB will cause the atoms to 'run aground' and coat the PCB. A Strontium coating of the PCB would undoubtedly lead to a short circuit. The simulation fell down at this point, it showed all atoms, over all variations in PCB, travelling into and below the PCB.

The next simulation details how the velocity of an atom might change if it were subjected to these time-dependent electric fields. The starting velocity for all atoms was 350ms^{-1}. Figure 17 shows the velocity distributions over Hogans time dependent fields. If the simulation was spot on it would show a constant deceleration. However the travelling speed of the electric potentials and the atom have not been synced up, leading to a choppy deceleration. The simulation for our PCB shows quiet an erratic velocity pattern.

The PCB design could prove the concept and it is an effective way to produce 10 sets of electrodes in a small space, even if quite expensive. The most evident improvement that could be made would be if six or more connections could be made to a series of electrodes and travelling potentials implemented.

5. Summary and Look Forward

A system was designed which, when constructed and evacuated should take hot ^{88}Sr atoms from dispensing to decelerated. The first step after dispensing would be excitation via two photon excitation using a blue 461nm laser to reach their first excited state and then a violet 413nm laser to scan higher Rydberg states at around $n = 50$. The exact Rydberg state would depend on how well the lasers were locked and the resolution of signal produced. Although fluorescence was seen in the process of frequency locking and a fluorescence signal was detected, no further progress was made in

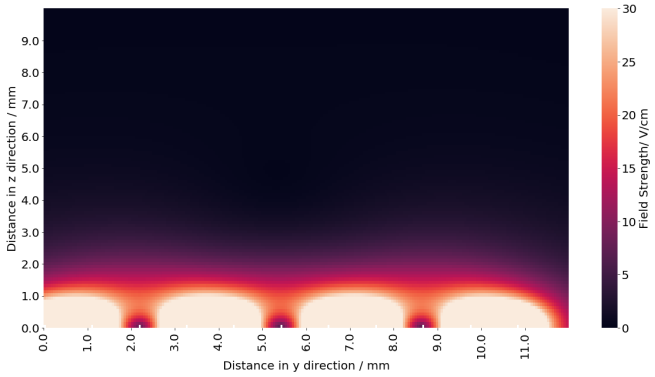

Fig. 14. Electric field above Hogan's PCB at 30 V, side view

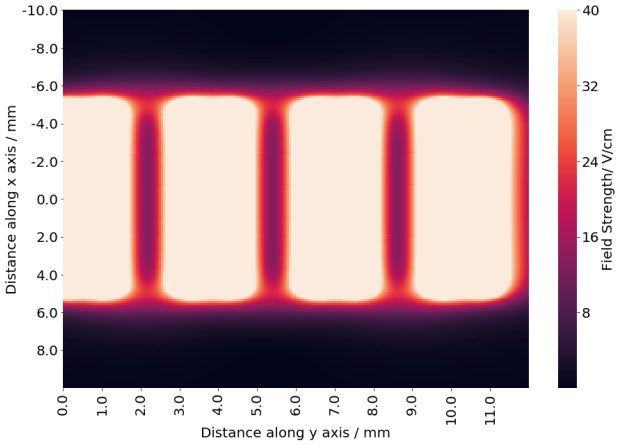

Fig. 15. Electric field above Hogan's PCB at 30 V, plan view

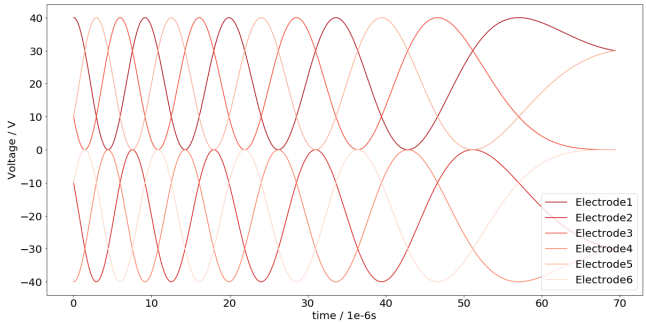

Fig. 16. Six oscillating potentials applied to electrodes 1-6 and then repeated.

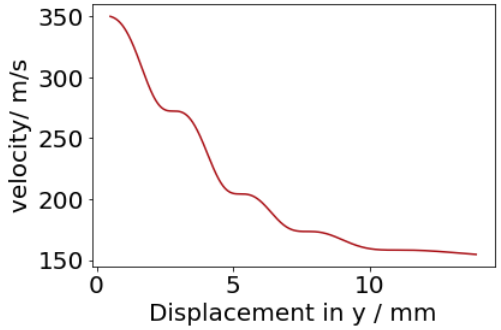

Fig. 17. The velocity distribution of one ^{88}Sr atom over Hogan's PCB

saturated absorption spectroscopy or EIT. Progression in this area could be achieved by further investigation of signal amplification and noise reduction techniques to try to achieve SASpect.

For the second step, deceleration, a PCB for a surface-electrode decelerator was designed and procured. Simulations were inconclusive. They showed good potentials existing above the PCB but hinted at issues with the flight path of the decelerated atoms themselves. The simulations could be taken forward by simulating a Gaussian distribution of atom velocities passing over the PCB. The PCB itself could be taken forward by developing a six connection, or similar, electrode setup to allow the use of multiple time dependent potentials. The spectroscopy, excitation and deceleration steps fit into a monolithic cell housing. This system acts as a good prototype to test the overarching concept of portable Rydberg-Stark deceleration. Although all parts arrived, not enough time was left to assemble the system and evacuate. This part of the project could be developed in the future by amending the thin edges which lead to gaps in the structure. The use of titanium as the primary material should also be considered.

6. Acknowledgements

I would like to thank Yogi and Yeshpal for their continual guidance throughout the year, without them this project would never have been possible. I would also like to thank Farzad for his calm nature and helpfulness, especially in creating the design of the PCB with me. I would also like to thank David, Johnny, Rustin, Alok and Jonathan for continually being friendly faces and sharing their lab space with us. Finally, a massive thanks to my lab partner Ed for taking on the practical spectroscopy side of the project, taking the lead on the simulations and for generally sharing this project with me.

REFERENCES

[1] Shuman E.S., Barry J.F., DeMille D., Laser cooling of a diatomic molecule. Nature 467, 820, 2010

[2] Liu J., Sprecher D., Jungen Ch., Ubachs W., Merkt F., Determination of the ionization and dissociation energies of the deuterium molecule (D2), Journal of Chemical Physics, 132, 154301, 2010

[3] Merkt F., Osterwalder A., Millimeter wave spectroscopy of high Rydberg states, Journal of Physical Chemistry, 121, 11810, 2004

[4] SI Brochure: The International System of Units (SI), Section 2.1.1.3, Unit of time (second), 8th edition, 2006, updated in 2014

[5] Santra R., Arimondo E., Ido T., Greene C.H., Ye J., High-Accuracy Optical Clock via Three-Level Coherence in Neutral Bosonic SR88, Physical Review Letters 94, 173002, 2005

[6] Dubè P., Madej A.A., Shiner A., Jian B., 88Sr+ single-ion optical clock with a stability approaching the quantum projection noise limit, Physical Review A 92, 042119, 2015

[7] Allan D.W., Ashby N., Hodge C.C., The Science of Timekeeping, Application Note 1289, Hewlett Packard, 2012

[8] Fulton R., Bishop A.I., Barker P.F., Optical Stark decelerator for molecules. Physical Review Letters 93, 243004, 2004

[9] Zeeman P., The Effect of Magnetisation on the Nature of Light Emitted by a Substance, Nature, 55, 1424, 1897

[10] Stark J., Observations of the effect of the electric field on spectral lines I. Transverse effect, Annalen der Physik, 43, 965983, 1914

[11] Rydberg J.R., Uber den Bau der Linienspektren der chemischen Grundstoffe, Zeitschrift fr Physikalische Chemie, 5, 227, 1890

[12] Rydberg J.R., Researches sur la constitution des spectres d'mission des lments chimiques, Kongliga Svenska Vetenskaps-Akademiens Handlingar, 2nd series, 23 (11): 1177, 1889

[13] Constantine E. Theodosiou, Lifetimes of alkali-metal atom Rydberg states, Physical Review A, Volume 30, Number 6, 1984

[14] Zimmerman M.L., Littman M.G., Kash M.M., Kleppner D., Stark structure of the Rydberg states of alkali-metal atoms, Physical Review A, Volume 20, Number 6, 1979

[15] Dunning F.B., Recent advances in Rydberg physics using alkaline-earth atoms, Journal of Physics B: Atomic, Molecular and Optical Physics, 49 112003, 2016

[16] Lochhead G., Excited state spatial distributions in a cold strontium gas, Durham theses, Durham University, 2012

[17] Millen J., A cold strontium Rydberg gas, Durham theses, Durham University, 2011

[18] Kim, J.B., Kong H.J., and Lee S.S., Laser frequency stabilization using a balanced bi-polarimeter, Applied Physics Letters 52, 417, 1988

[19] Lancaster G.P.T., Conroy R.S., Clifford M. A., Arlt J., and Dholakia K., Optics Communications, 170, 79, 1999

[20] Wieman, C. and Hänsch, T.W., Doppler-Free Laser Polarization Spectroscopy, Physical Review Letters, 36, 1170-1173, 1976

[21] Holt R.A., Scholl T.J., Rosner S.D., Laser-rf saturation spectroscopy: A novel fast-ion-beam sub-Doppler method, Canadian Journal of Physics, 75, 10, 721-732, 2011

[22] Preston D.W., Doppler-free saturated absorption: Laser spectroscopy, American Journal of Physics, 64, 11, 1432-1436, 1996

[23] Sigg D., Printed Circuit Boards for Ultra High Vacuum, Document LIGO-T060280-x0, https://dcc.ligo.org/LIGO-T060280/public, 2007

[24] Introduction to vacuum technology, fundamentals, conductance, Formula 1-30, https://www.pfeiffer-vacuum.com/en/know-how/introduction-to-vacuum-technology/fundamentals/conductance/

[25] Townsend D, Goodgame A.L., Procter S.R., Mackenzie S.R., Softley T.P., Deflection of krypton Rydberg atoms in the field of an electric dipole, Journal of Physics B: Atomic, Molecular and Optical Physics, 34, 439-450, 2001

[26] Vliegen E., Wörner H.J., Softley T.P., Merkt F.: Nonhydrogenic effects in the deceleration of Rydberg atoms in inhomogeneous electric fields, Physical Review Letters, 92, 033005, 2004

[27] Vliegen E., Hogan S.D., Schmutz H., Merkt F., Stark deceleration and trapping of hydrogen Rydberg atoms, Physical Review A, 76, 023405, 2007

[28] Hogan, S.D., Merkt, F. Demonstration of three-dimensional electrostatic trapping of state-selected Rydberg atoms, Physical Review Letter 100, 043001, 2008

[29] Seiler C., Hogan S.D., Schmutz H., Agner J.A, Merkt F., Collisional and Radiative Processes in Adiabatic Deceleration, Deflection, and Off-Axis Trapping of a Rydberg Atom Beam, Physical Review Letters, 106, 073003, 2011

[30] Rogers Corperation, R4000 series data sheet, https://www.rogerscorp.com/documents/726/acs/RO4000-Laminates-RO4003C-and-RO4350BData-Sheet.pdf

[31] Hogan, S.D., Allmendinger, P., Saßmannshausen, H., Schmutz, H., Merkt, F., Surface-electrode Rydberg-Stark decelerator, Physical Review Letter 108, 063008, 2012

[32] Meek S.A., Bethlem H.L., Conrad H., Meijer G., Trapping molecules on a chip in travelling potential wells, Physical Review Letter 100, 153003, 2008

[33] Groswasser D., Waxman A., Givon M., Aviv G., Japha Y., Keil M., Folman R., Retroreflecting polarization spectroscopy enabling miniaturization, Review of Scientific Instruments, 80, 093103, 2009

APPENDIX

I. Full Vacuum Set Up

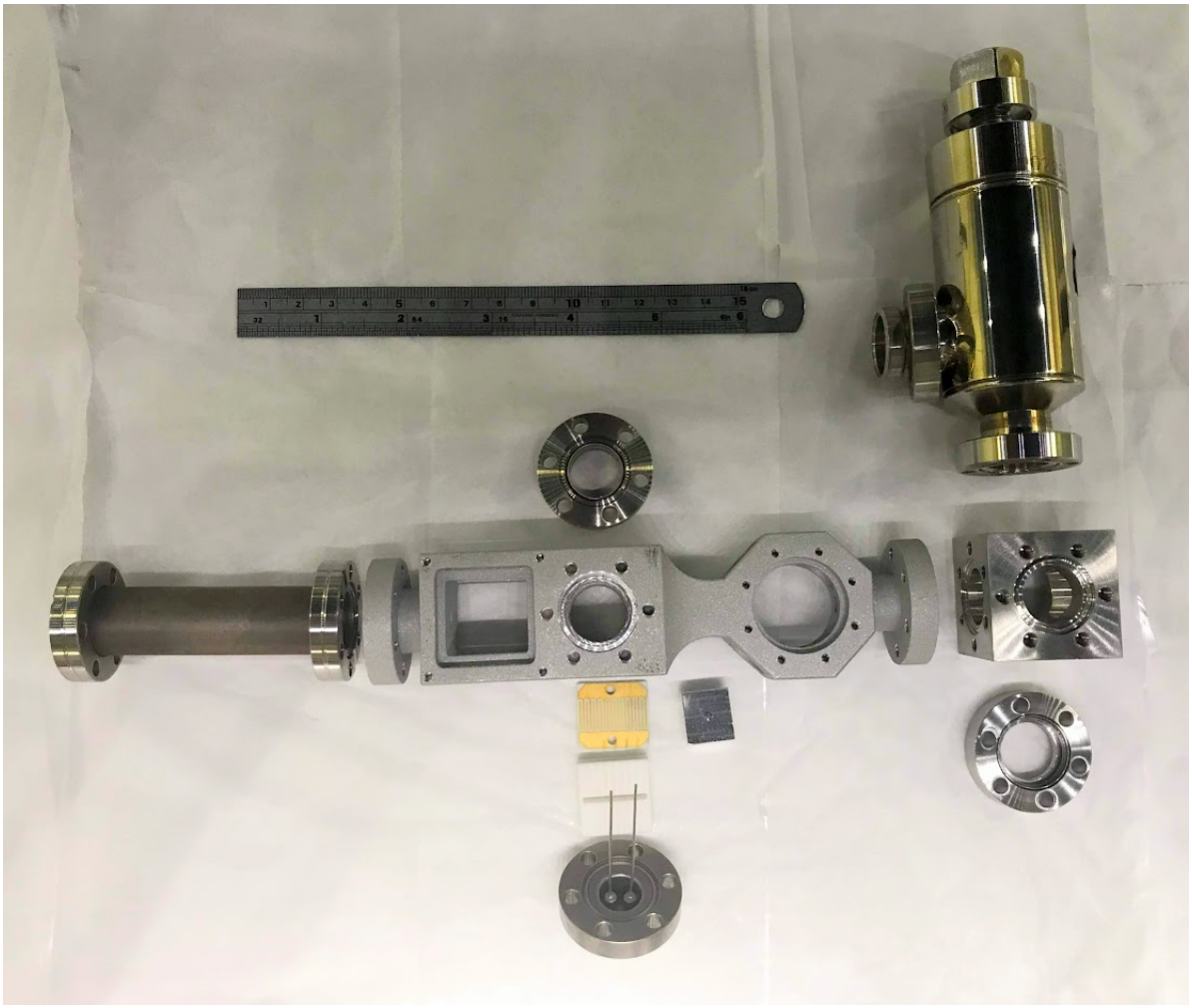

Fig. 18. An exploded view of the vacuum set up.

II. Monolithic Cell

Fig. 19. Monolithic cell, Physical copy

III. PCB

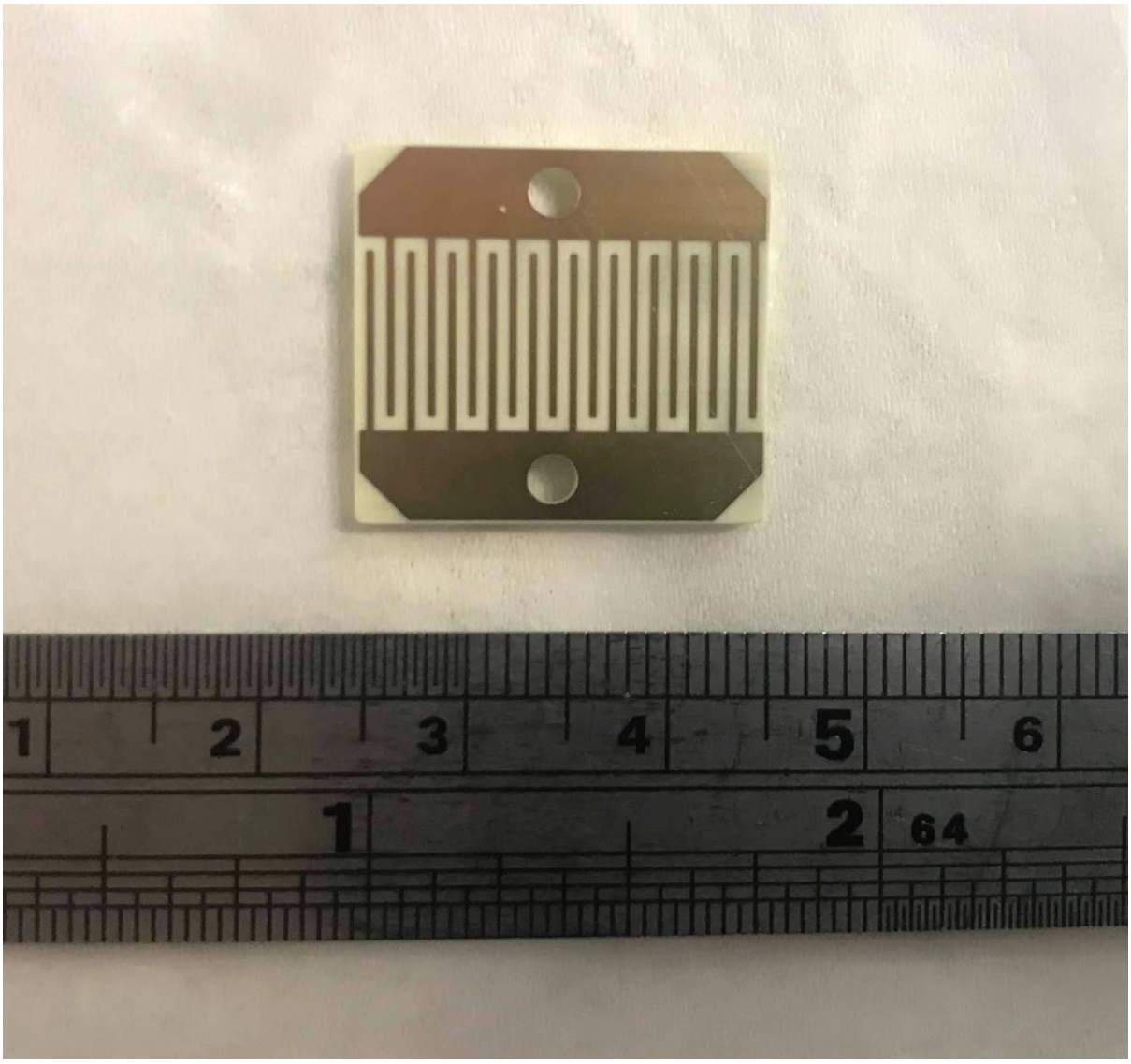

Fig. 20. Finished product, made from RO4350b, gold electrodes with no silkscreen or soldermask.

IV. Differential Pumping Insert

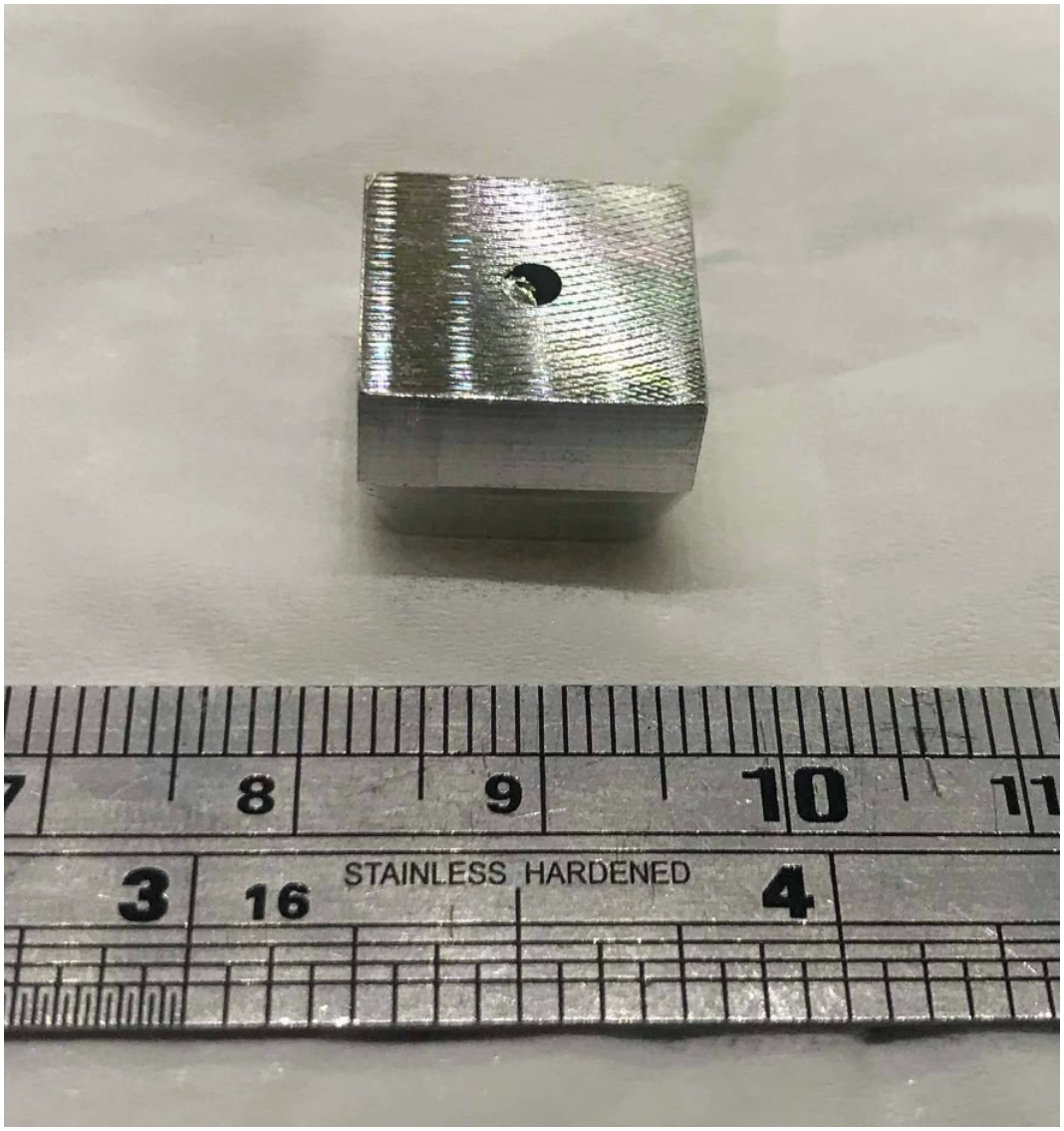

Fig. 21. Differential pumping insert to be Torr sealed in.

V. Fluorescence

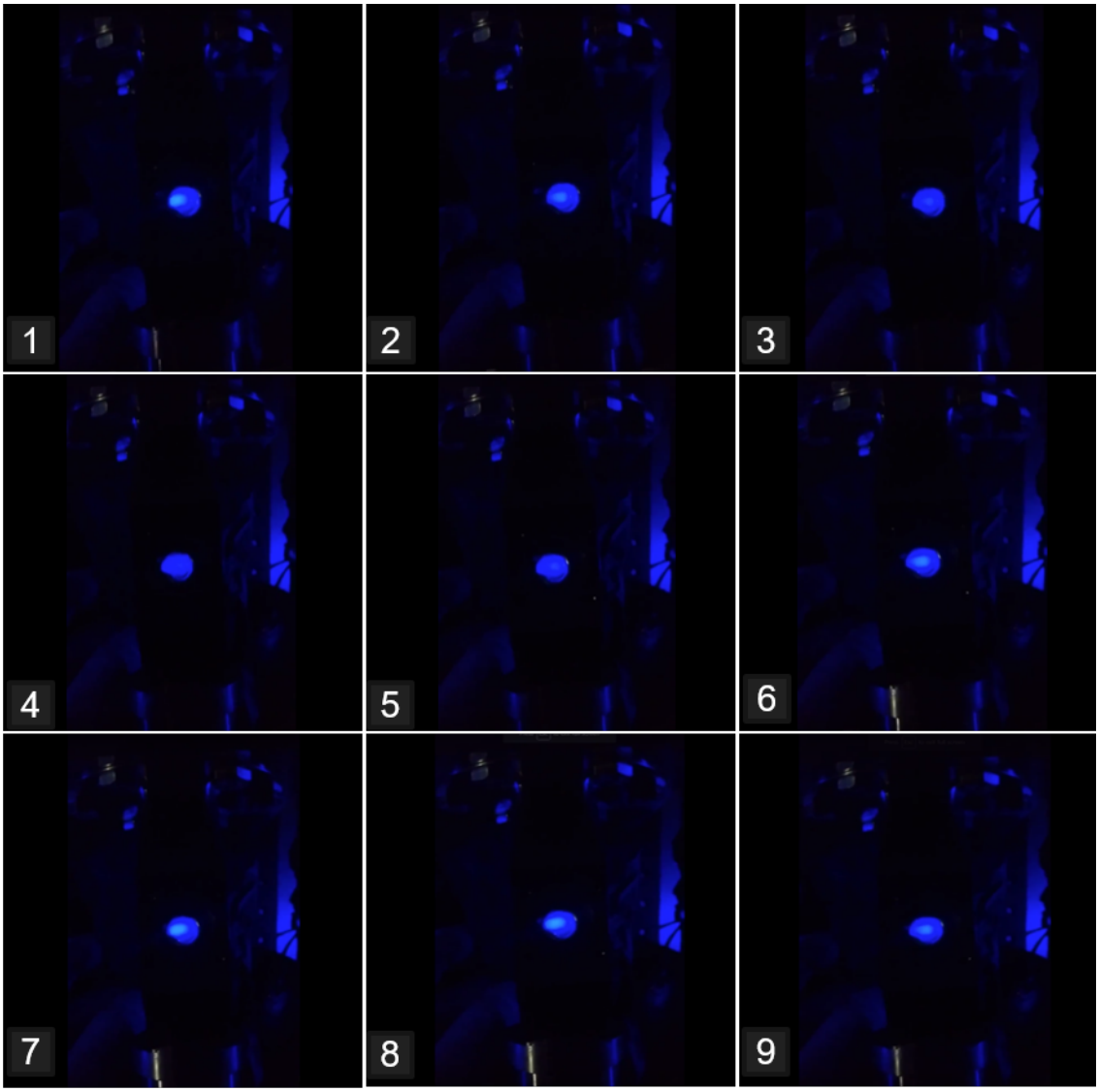

Fig. 22. A set of frames from a video of fluorescence. The time between each frame is approximately 0.23 seconds. The laser was set to scan over the resonant frequency. As a result the fluorescencef fades in and out. Frames 1, 7 and 8 show the resultant fluorescence while the laser is on resonance.

VI. Optical Set Up

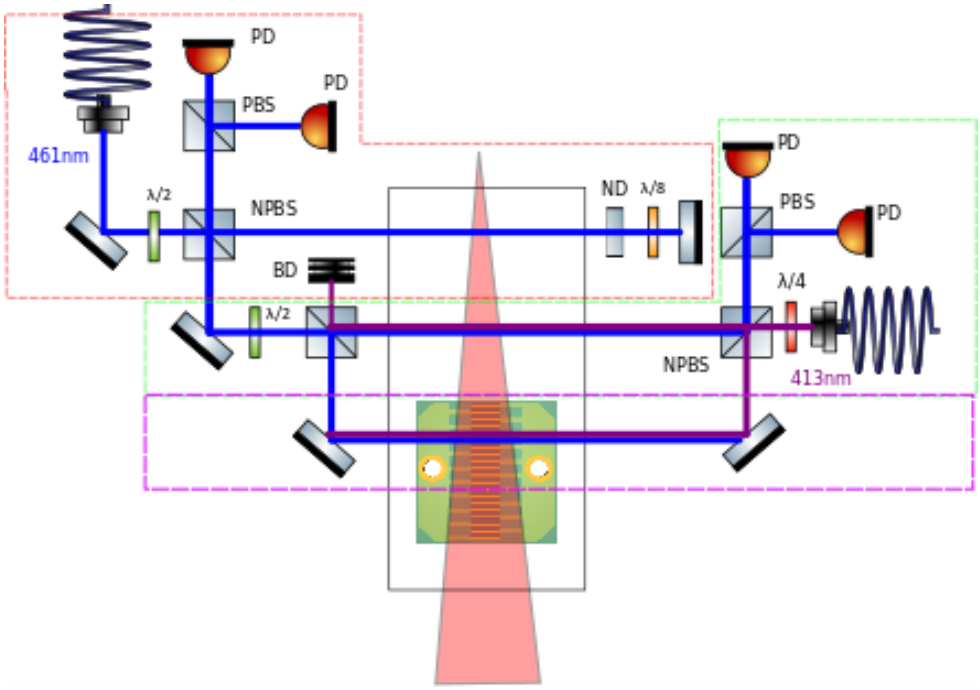

Fig. 23. Full intended optical arrangement schematic.

VII. Vacuum Set Up

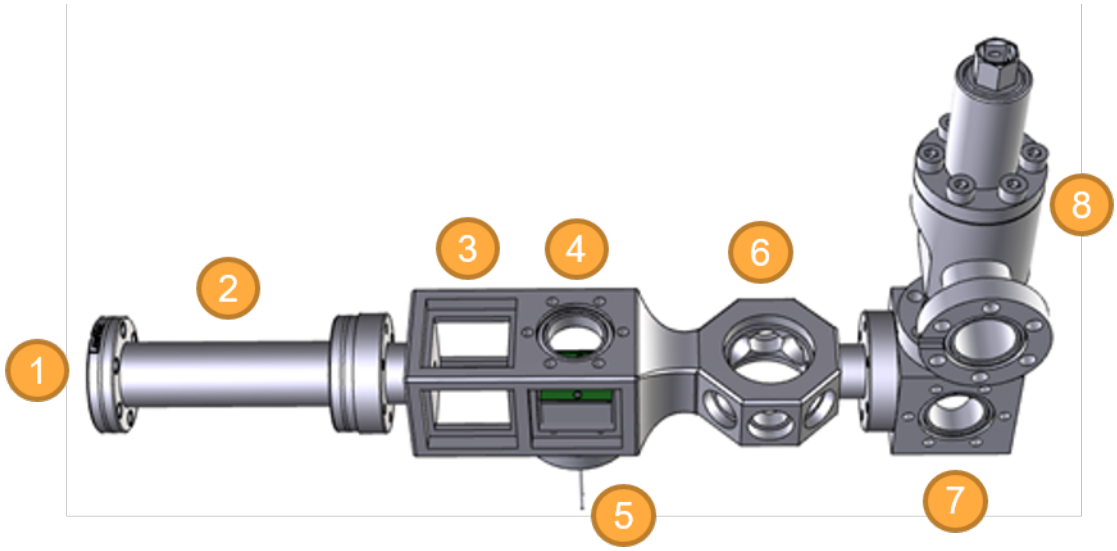

Fig. 24. Experimental setup, picture from Inventor assembly. 1- ^{88}Sr entrance point; 2- CF16 nipple; 3- spectroscopy stage; 4- PCB housing/ deceleration stage; 5- electrical feedthrough; 6- trapping/ velocity measurement stage; 7- six way cube; 8- All-metal valve.